DEVELOPMENT OF INTERMITTENT LAYER HEIGHT CONTROL USING LINE SCANNING FOR SUCCESSIVE TOOLPATH ADAPTION IN LASER MATERIAL DEPOSITION

Jan Bremer[1], Tim Fleischhauer[1], Andres Gasser[1], Johannes Henrich Schleifenbaum[1,2]

1: Fraunhofer Institute for Laser Technology
2: RWTH Aachen University – Digital Additive Production
Aachen, Germany

ABSTRACT

Laser Material Deposition (LMD), also known as Directed Energy Deposition (DED), is an additive manufacturing (AM) technology used in repair and manufacturing applications of high-value components. It is commonly used in industries such as aerospace, tooling and turbomachinery. The ability to produce near-net-shape parts results in low material losses and can lead to reduction of production costs and lead times compared to conventional machining processes. In hybrid manufacturing, LMD is used together with conventional processes to exploit both technologies' benefits for production of large parts with complex structures. Increasing stability and geometric accuracy of LMD processes is key enabler for further expansion of applications of this manufacturing technology. Current approaches focus on parameter studies, development of predictive modeling as well as closed-loop control. This work proposes a novel approach for component geometry control in LMD. This approach is based on an intermittent geometry control. LMD builds are split into separate sections. After depositing a section or block, a laser line scanner is utilized to measure the detected block geometry in the form of a point cloud. An algorithm is developed that calculates local height deviations from target geometry and adjusts the feed rate along the tool center point (TCP) path. Experiments are conducted in order to establish control parameters such as reference distance between adjacent support points along the TCP path (minimum and maximum feed rate increment) and functional relation between layer height and feed rate. Thus, dependence of layer height with respect to absolute part height is investigated.

Keywords: Laser Material Deposition, Directed Energy Deposition, laser line scanner, adaptive processing, layer-height-control, point cloud manipulation
Corresponding author: Jan Bremer

1. INTRODUCTION

Production of high performance and lightweight components is a crucial task in industries such as aerospace or automotive. They play a key role in terms of sustainability and performance enhancement. In manufacturing of metal components in aerospace applications, state of the art conventional machining processes come with high buy-to-fly ratios, i.e. huge ratios between the weights of raw material used to produce components compared to the weights of the final parts. Up to 90% of the raw material is wasted [1]. Correspondingly, high production costs occur, resulting from the usage of high-value materials such as titanium alloys or Ni-based superalloys. [2, 3]

Combining conventional manufacturing processes with additive manufacturing (AM), so-called hybrid manufacturing, yields considerable improvements compared to sole conventional manufacturing. One of the commonly used AM technologies is Laser Material Deposition (LMD). It offers the potential to manufacture complex forms and near-net-shape parts, resulting in significantly reduced production costs and lead times, as well as energy and raw material savings. [3, 4]

LMD is an AM technology where energy emitted from a laser source is utilized to locally melt a substrate. Filler material in the form of powder or wire is transported into the melt pool. Powder is carried by an inert gas jet. The melt pool is shielded by an additional inert gas jet. After solidification, the filler material forms a track on the substrate. Layers of material are formed by the deposition of multiple tracks. After depositing a layer, the relative distance between cladding head and substrate is increased by an estimated layer height. [5]

If the estimated layer height differs from the deposited layer height beyond certain limits, the process becomes unstable and must be aborted. Investigations into control strategies of the deposited layer height are conducted to increase process stability and geometrical accuracy.

To control the deposited layer height in a wire LMD (WLMD) process, *Garmendia et al.* [6] propose to use the feed rate as the actuating variable. A stationary structured light geometry scanner is utilized to measure each deposited layer. The deposition process is interrupted for measuring. Subsequently, the feed rate of the next layer is adjusted locally to deviations between the estimated and the deposited layer height along the tool center point (TCP) path. A functional relation between feed rate and layer height is established experimentally for this purpose. [6]

Depositing a certain number of layers blockwise and iteratively recalculating the number of layers to be deposited in a subsequent block is another approach to layer height control. Block height is measured with a stationary structured light sensor after deposition. Recalculation is then based on differences between measured block height and estimated block height. [7]

Another approach to control layer height is to adjust the average layer height of the following block based on the measurement of the previously deposited block. Again, a structured light sensor is used. [8]

Further investigations in controlling the deposited height include adjusting laser power [9] or feed rate [10] based on charge couple device (CCD) cameras. A laser line scanner (LLS) is utilized by *Heralić et al.* [11] to measure layer height and subsequently adjust wire feed rate in a WLMD process. Powder feed rate has a considerable influence on track height [12]. However, it is rarely considered in height control because of its comparatively long response time [12, 13]. Several guidelines for stable line scanning results, such as the use of LLS with a wavelength ranging from 405 nm to 520 nm or the sandblasting of substrates, are recommended. [14]

The algorithm presented in this paper is based on the work of *Garmendia et al.* [6]. Novel is the approach to use a LLS to measure the height of deposited blocks. The control algorithm is improved in terms of selecting measurement points to calculate local height deviations and experimentally determining boundary conditions for the feed rate adjustments based on the capabilities of the used LMD system.

2. EXPERIMENTAL SETUP

2.1 System setup

Experiments are conducted on a LMD system consisting of a 90kg payload industrial robot and a variable beam geometry powder processing optic. A continuous coaxial powder delivery nozzle is used. Beam source is a diode laser with maximum power output of 5000W and a wavelength of 940 – 1060 ± 10 nm. A line scanner with a nominal measuring line width of 100 mm and a wavelength of 405 nm is used. The system setup is depicted in Figure 1.

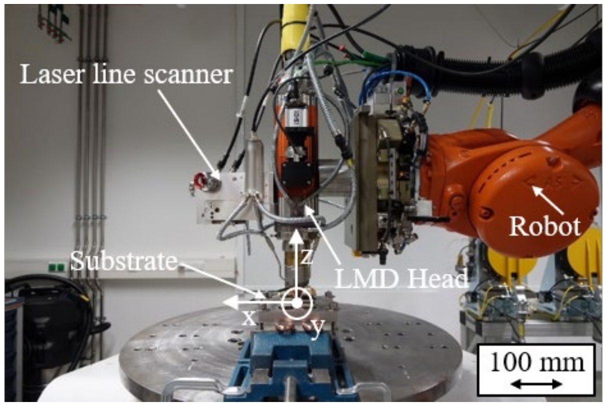

Figure 1. System setup

Plasma atomized Inconel 718 powder with a grain size distribution ranging from 15 to 45 µm is used. Chemical composition is depicted in table 1.

Table 1. Chemical Composition of Inconel 718

Element	Cr	Co	Fe	Mo	Ni	Nb	Ta	Ti
Mass fraction [%]	17 - 21	0 - 1	13 - 25	2.8 - 3.3	50 - 55	4.75 - 5.5	0 - 0.05	0.65 - 1.15

2.2 Process parameters

All measurements are conducted using the process parameters listed in table 2. Nominal feed rate is 33.3 mm/s. Feed rate variations in experiments and within the height control strategy are always denoted as deviation percentages from the nominal feed rate.

Table 2. Process parameters

Parameter	**Value**
Feed rate	33.3 mm/s
Laser power	1000 W
Beam diameter	1.6 mm
Powder feed rate	9.5 g/min
Powder delivery gas	3.5 NL/min

Parameter	**Value**
Powder focus offset	-1 mm
Shielding gas flow rate	10.7 NL/min
Track Overlap	50%
Estimated layer height	0.65 mm

2.3 Measurement technologies

A LLS measures two-dimensional height profiles by utilizing the light section principle. Three-dimensional scanning of an object is achieved by concatenating height profiles obtained at a fixed

frequency whilst scanner and object are moved relative to each other. In this work, height profiles are measured at a frequency of 83.3 Hz. Resolution of the scan line is 1280 points which yields a distance of 78 µm between adjacent points on a nominal scan line of 100 mm. Smallest height difference between adjacent points is 12 µm for the given configuration. A line scanning software is used to acquire and synchronize line scanning and machine data, resulting in output of a point cloud of the scanned geometry in the working coordinate system.
To evaluate feed rate limits considered for the height control strategy, a laser tracker is used. The laser tracker measures positions of a retroreflector attached to the processing optics at a fixed frequency of 1000 Hz. Measurement of positions is afflicted with an error of maximum ±27 µm for the given system setup.

2.4 Height control strategy

The approach investigated in this work is to deposit a fixed number of layers within a single block. After depositing a block, block height is measured with the LLS and local deviations from the estimated height are calculated. The TCP path is split into segments to adjust the feed rate locally with respect to local height deviations. Each segment is assigned a local feed rate. If local height deviations Δh_{local} stay within desired stability limits, it is assumed that adjusting the feed rate is sufficient to compensate them. Stability limits are set according to equation 1. The next block is deposited with locally adjusted feed rates. If local height deviations exceed stability limits, the current LMD process is aborted. Layer heights are recalculated based on the current height and a new LMD process is started, following the same control strategy. The principle of the height control strategy is depicted in Figure 2.

$$-1\text{ mm} \leq \Delta h_{local} = h_{set} - h_{local} \leq 3\text{ mm} \qquad (1)$$

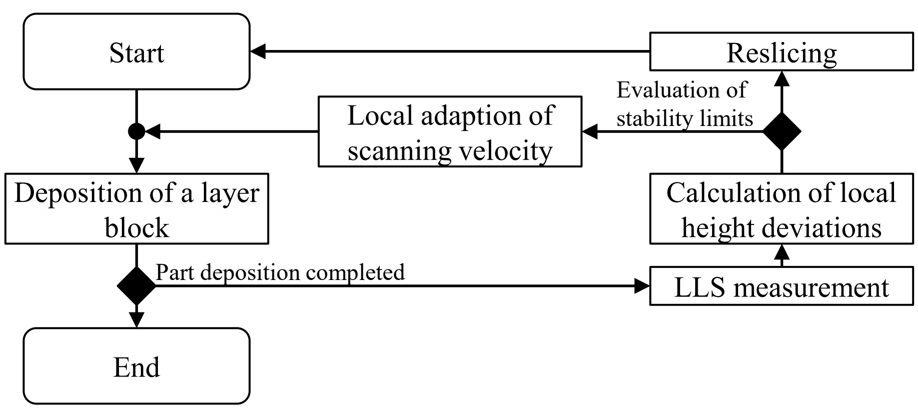

Figure 2. Principle of the height control strategy

Initially within the height control strategy each section of the path, where material is deposited, is split into segments. These sections are framed by discrete points $P_S = (x_S, y_S, z_S)^T$ and $P_E = (x_E, y_E, z_E)^T$, as depicted in Figure 3a. In this work, curved trajectories are approximated by linear sections.

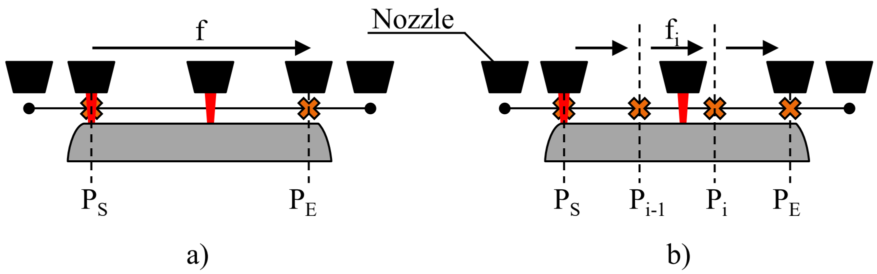

Figure 3. Preparation of a TCP path for application of the height control strategy
a) Given TCP path
b) TCP path with support points

To interpolate the path from P_s to P_E with support points P_i as depicted in Figure 3b, a normalized direction vector n_{line} is calculated with equation 2.

$$n_{line} = \begin{pmatrix} x_E - x_S \\ y_E - y_S \\ z_E - z_S \end{pmatrix} \cdot \frac{1}{\sqrt{(x_E - x_S)^2 + \left(y_E - y_S\right)^2 + (z_E - z_S)^2}} \tag{2}$$

A reference distance Δs, used to calculate the number of support points to be placed between P_S and P_E, must be established experimentally. The number of support points can then be calculated with equation 3, where $d(P_S, P_E)$ is the euclidean distance between two points and $\lfloor x \rfloor$ is the rounding off function for a value x.

$$n = \left\lfloor \frac{d(P_S, P_E)}{\Delta s} \right\rfloor \tag{3}$$

Since the number of support points is rounded, the effective distance Δs_{eff} between support points is subsequently calculated with equation 4. By rounding off it is assured that the effective distance Δs_{eff} between two support points is always larger than the reference distance Δs.

$$\Delta s_{eff} = \frac{d(P_S, P_E)}{n} \tag{4}$$

The distance between P_S and P_E is filled with support points according to equation 5.

$$P_i = P_S + n_{line} \cdot \Delta s_{eff} \cdot i \qquad i = 1 \ldots n_{line} \tag{5}$$

The LLS measurement of the deposited surface yields data in the form of a three-dimensional point cloud C^{LLS}. For each support point P_i, a set C_i^{LLS} of point cloud points $P_k^{LLS} = \left(x_k^{LLS}, y_k^{LLS}, z_k^{LLS}\right)^T$ is determined that lies within a certain influence area. The influence area is defined as a rectangle ranging from P_{i-1} to P_i, thus having an edge length in the direction of the normalized direction vector n_{line} of Δs_{eff}. Perpendicular to n_{line}, the edge length is set to the beam diameter d. To determine, whether a point P_k^{LLS} lies within the influence area of a support point P_i, distance vector r_{i-1} in the x-y-plane is calculated with equation 6.

$$r_{i-1} = \begin{pmatrix} x_k^{LLS} \\ y_k^{LLS} \end{pmatrix} - \begin{pmatrix} x_{i-1} \\ y_{i-1} \end{pmatrix} \quad (6)$$

Transformation from the global x-y-coordinate system representation r_{i-1} into a local $\tilde{x}$-$\tilde{y}$-coordinate system representation $\tilde{r}_{i-1} = (\tilde{x}_{i-1}, \tilde{y}_{i-1})^T$ is conducted with equation 7 for simplifying the determination.

$$\tilde{r}_{i-1} = \begin{bmatrix} -\sin(\alpha) & -\cos(\alpha) \\ -\cos(\alpha) & \sin(\alpha) \end{bmatrix} \cdot r_{i-1} \quad (7)$$

Orientation angle α is calculated with equation 8.

$$\alpha = \cos^{-1}\left(n_{line} \cdot \begin{pmatrix} 0 \\ 1 \\ 0 \end{pmatrix} \right) \quad (8)$$

An exemplary influence area is given in Figure 4.

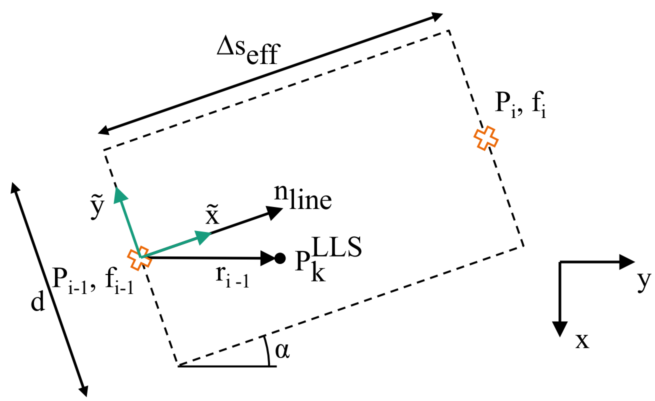

Figure 4. Influence area for a support point P_i

Determination of the set C_i^{LLS} of all point cloud points that belong to the influence area of a given support point P_i leads to evaluating equation 9 for each point of the point cloud.

$$C_i^{LLS} = \left\{ P_k^{LLS} \in C^{LLS} : 0 \le \tilde{x}_{i-1} \le \Delta s_{eff,i} \wedge -\frac{d}{2} \le \tilde{y}_{i-1} \le \frac{d}{2} \right\} \quad k = 0 \ldots \left| C^{LLS} \right| \quad (9)$$

Local height at a support point P_i is calculated with equation 10.

$$h_{local,i} = \frac{1}{\left| C_i^{LLS} \right|} \cdot \sum_{P_k^{LLS} \in C_i^{LLS}} z_k^{LLS} \quad (10)$$

From the difference $\Delta h_{local,i} = h_{set} - h_{local,i}$ between the estimated height h_{set} and the deposited height $h_{local,i}$ a local adaption of the feed rate f_i is conducted based on a functional relation

$f_i = f(\Delta h_{local,i})$. The functional relation is determined experimentally in this work. A visualization of the above described interaction of TCP path and point cloud data is depicted in Figure 5.

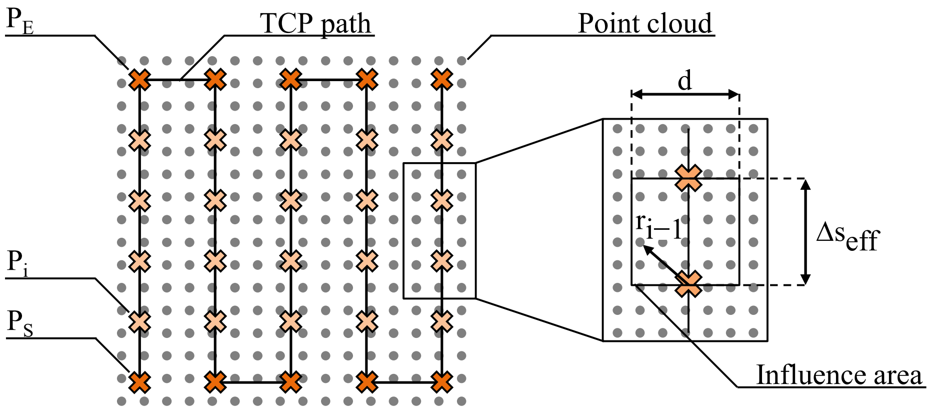

Figure 5. Overlapping of TCP path and point cloud data

Due to the nature of the experimental setup, the alignment of point cloud measurements with the nominal CAD model used for comparison as well as the LLS measurements can contain errors. Reasons can be, among others, geometrical tolerances in the mounting of the LLS, latency in triggering of LLS measurements in the control system as well as errors in LLS tool data in the control system and misalignment of the specimens due to mounting errors.

A Random Sample Consensus (RANSAC) algorithm is used to compensate tilting of the point cloud. RANSAC is a non-deterministic, iterative algorithm, used to fit a model to data that is heavily disturbed by outliers. [15]

In this work, the RANSAC algorithm is implemented to estimate the substrate plane in the given point cloud data. Height of a point is then calculated as projected distance from the estimated plane, resulting in a height profile of a deposited object. In Figure 6 an exemplary height profile calculation is depicted. Deposited object is a cuboid with an edge length of 25 mm and an estimated height of 15 mm.

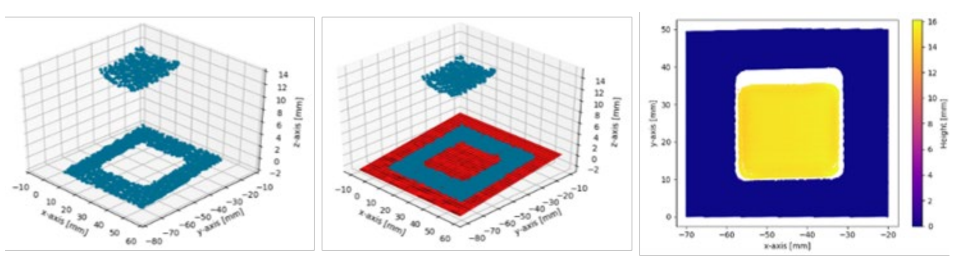

a) b) c)

Figure 6. Application of the RANSAC algorithm

a) Raw point cloud

b) Estimated substrate plane

c) Height profile

After tilting compensation with the RANSAC algorithm, absolute position errors are compensated. The center point of all height profile points whose height exceeds a tolerance band around the

value zero is calculated. Each point of the point cloud is shifted by the distance between the calculated center point and the geometrical center point, obtained from the Computer Aided Design (CAD) data of the deposited object.
The height control strategy is implemented as a Python script, utilizing the NumPy module.

2.5 Experimental investigations

To implement the height control strategy on the LMD system, several parameters and relations must be determined experimentally. Four experiments are conducted to establish a reference distance Δs as well as a maximum and minimum feed rate increment between adjacent support points and a functional relation between layer height and feed rate.

Experiment 1
Linear TCP paths of 25 mm length are examined at different feed rates to investigate, whether actual feed rates can meet required set feed rates within an interval of ±50% around the nominal feed rate. Smallest feed rate increments investigated are 1% steps within an interval of ±5% around the nominal feed rate. Each measurement is repeated three times. Measurements are conducted in the x-direction as well as the y-direction of the base coordinate system, depicted in Figure 1. TCP positions are measured at distinct points in time using the laser tracker system. Feed rate is calculated from obtained position data.

Experiment 2
Reference distance Δs between two adjacent support points with respect to a maximum feed rate increment is established by examining a TCP path as depicted in Figure 7. A linear TCP path is filled with support points at a fixed distance Δs. Distinct distance values 0.5 mm, 1 mm, 2 mm, 3 mm, 5 mm and 10 mm are investigated. Feed rate is varied stepwise in increments ranging from $f_{Nom} \cdot (1 - 3\Delta f)$ to $f_{Nom} \cdot (1 + 3\Delta f)$, with Δf describing fixed percentages 1%, 5% and 10%, respectively. The feed rate trajectory contains two maxima, resulting in 26 support points on the TCP path. A full factorial investigation of Δf and Δs is conducted. Each combination is repeated three times. TCP positions are measured at distinct points in time using the laser tracker system. Feed rate is calculated from obtained position data.

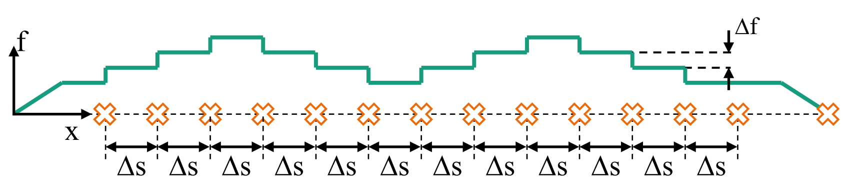

Figure 7. Experiment to establish a reference distance Δs

Experiment 3
Twelve cuboids, consisting of three blocks with eight layers each, are deposited at nominal feed rate. Block height is measured with the LLS to investigate nominal layer height, deposited with the process parameter set. Influence of the distance to the substrate plane on the deposited layer height is investigated. Build-up strategy consists of contour trajectories and hatch trajectories in the form of meanders, fly-in and fly-out paths are integrated.

Experiment 4

To determine a functional relation between layer height and feed rate, cuboids, consisting of three blocks with four layers each, are deposited at various feed rates. Block height is measured with the LLS. Layer height is calculated from block height measurements. Feed rate is varied within an interval of ±50% around nominal feed rate at increments of 10%. For each feed rate, three cuboids are deposited.

Experiment 5

Six cuboids are deposited in two steps for evaluation of the experimentally determined control parameters and functional relations implemented in the layer height control strategy. In the first step, tilted planes are deposited by decreasing the feed rate from the maximum feed rate limit to the minimum feed rate limit when moving the TCP in positive y-direction. Feed rate is decreased by the maximum feed rate increment Δf on segments with the length of the reference support point distance Δs. Tilted planes consist of four deposited layers each. In the second step, a block of four layers is deposited on top of each tilted plane. Layer height control is applied to the deposition process of three blocks. The remaining blocks are deposited without layer height control strategy as reference.

3. RESULTS

The capability of the LMD system to meet set feed rates is examined in experiment 1. Differences between measured actual feed rates f_{act} and set feed rates f_{set} are depicted in Figure 8. Set feed rates are denoted with either a letter M or P, indicating a negative or a positive deviation from the nominal feed rate, followed by a percentage value. For example, feed rate FM50 refers to a feed rate $f = f_{nom} \cdot (1 - 50/100)$.

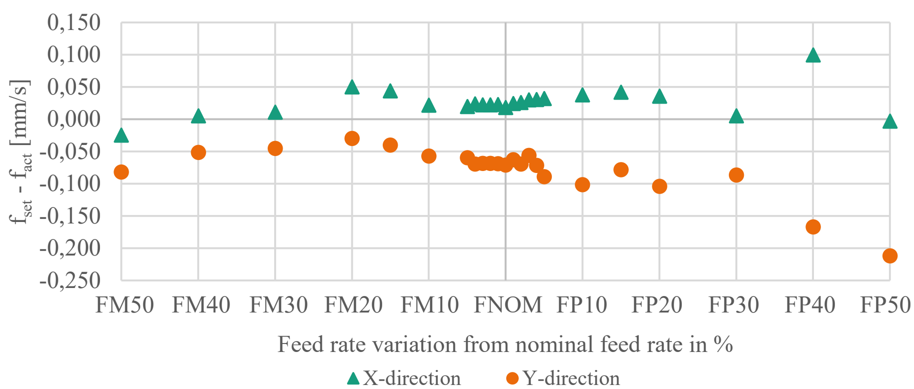

Figure 8. LMD system capabilities to meet set feed rates

Over the whole range of investigated feed rates, deviations from set feed rate lie within a limit of 0.21 mm/s. On average, deviations amount to 0.09% of the set feed rate in x-direction and 0.23% in y-direction. Maximum amount in x-direction is 0.21% at a feed rate variation of +40%, in y-direction 0.49% at a feed rate variation of -50%.

For implementation of the height control strategy it is hence assumed that the LMD system is capable of meeting required set feed rate. Even small feed rate variations of 1% can be distinguished. Therefore, no minimum feed rate increments are included in the height control strategy. Since deviations in x- and y-direction are of similar magnitude, possible influence of

direction is neglected in the following experiments. Isotropic behavior of the LMD system is assumed within the working space.
Stepwise variation of feed rate is applied on a TCP path in experiment 2 to investigate the influence of support point distance Δs in correlation with feed rate increment Δf on the feed rate accuracy. As depicted in Figure 9a, the LMD system cannot follow a stepwise variation of the set feed rate when the support point distance is set to 0.5 mm. Applying a support point distance of 10 mm yields an accurate actual feed rate profile, as depicted in Figure 9b. In the given example, a feed rate increment of 10% is used.

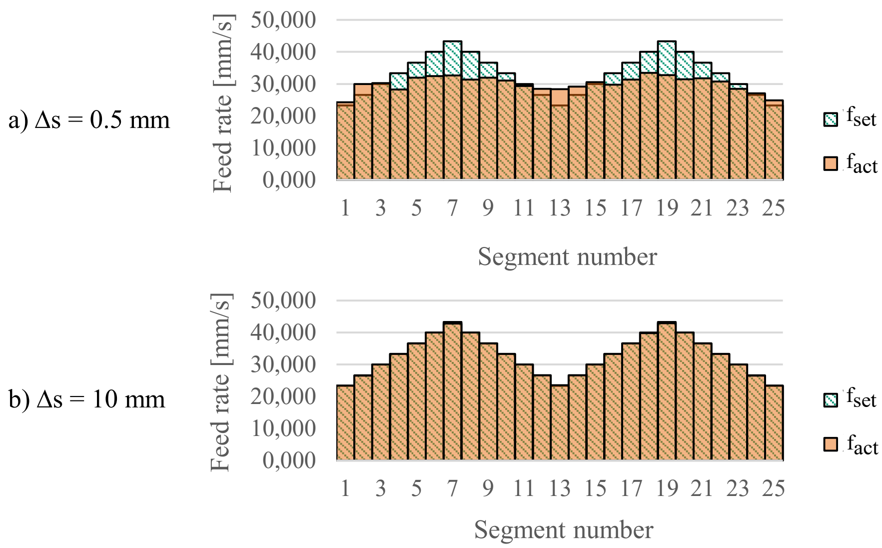

Figure 9. Comparison of the influence of support point distances on the feed rate accuracy

For quantification purposes, feed rate error $E_{\Delta s}^{\Delta f}$ is defined in equation 11. The feed rate error describes the ratio between the sum of the absolute values of all feed rate deviations, occurring on each line segment enclosed by two adjacent support points and the sum of the corresponding set fee rates.

$$E_{\Delta s}^{\Delta f} = \frac{\sum_{Seg} \left| f_{set,\, Seg} - f_{act,\, Seg} \right|}{\sum_{Seg} f_{set,\, Seg}} \cdot 100 \qquad (11)$$

Calculated feed rate error is depicted in Figure 10 for all investigated combinations of support point distance and feed rate increment. It decreases with increasing support point distance as well as with decreasing feed rate increment. Support point distances of more than 2 mm yield feed rate errors of less than 2% for all investigated feed rate increments.

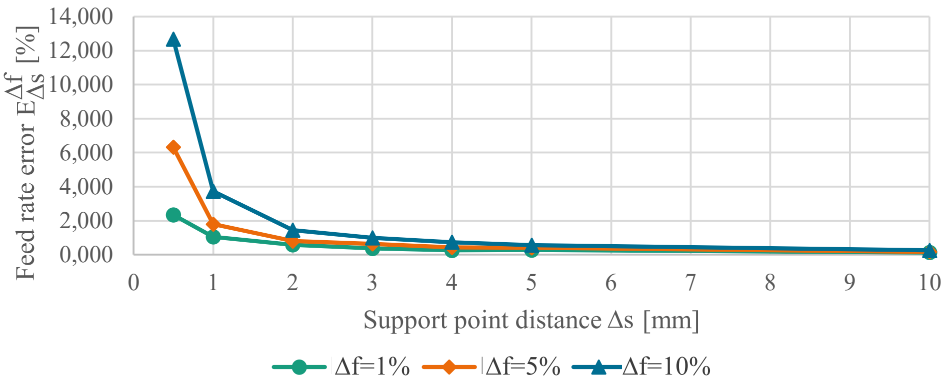

Figure 10. Evaluation of the feed rate error

For implementation in the height control strategy, a reference support point distance of 2 mm is chosen. A maximum feed rate increment for adjacent support points of 10% is implemented in the height control strategy.

In experiment 3, cuboids are deposited using the process parameter set and the nominal feed rate. Each cuboid consists of three blocks. After depositing a block, block height is measured with the LLS. Overall 36 blocks are deposited. An average block height of 4.97 mm is calculated with a standard deviation of 0.084 mm, resulting in a layer height of 0.621 mm which is slightly smaller than the 0.65 mm estimated layer height process parameter.

To investigate the influence of the distance from the substrate on the deposited layer height, deviation of the measured block height from the average block height is depicted as a box plot in Figure 11. Block height of the first block, deposited directly on the substrate, is, on average, 98% of the average block height. The third block, which is deposited at the largest distance from the substrate, amounts to 102% of the average block height. Standard deviation of the first block deposited is about one magnitude larger than of the remaining ones.

Since the block height deviates about only 4% within an absolute distance of 15 mm to the substrate, the influence of the distance from the substrate on the deposited layer height is neglected in the height control strategy.

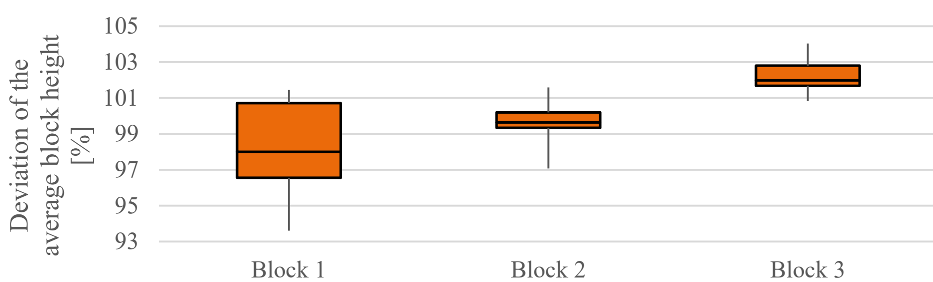

Figure 11. Box plot representation of deviations from the average block height

Functional relation between feed rate and layer height is investigated in experiment 4. Three cuboids, consisting of three blocks each, are deposited for each investigated feed rate, resulting in nine blocks to evaluate for each feed rate. A box plot representation of the block height distribution with respect to the feed rate is depicted in Figure 12.

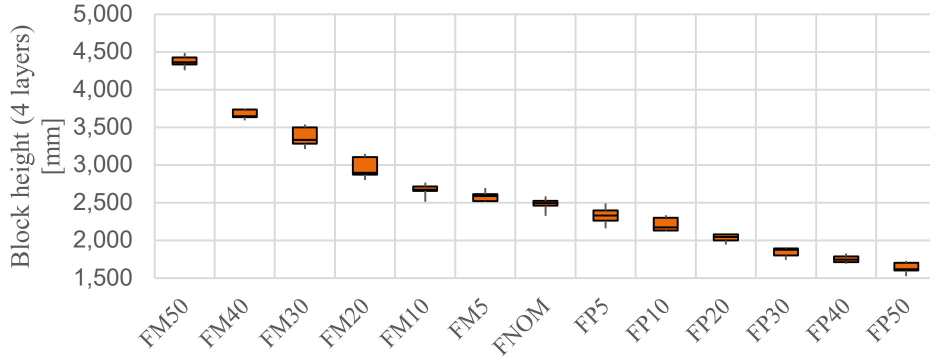

Figure 12. Box plot representation of the block height distribution with respect to the feed rate

Block height increases more with decreasing feed rates than it decreases with increasing feed rates. Linear regression is applied to the measurements in an area of ± 30% around the nominal feed rate, yielding a model equation (equation 12) with a R^2-value of 0.977.

$$h\ [mm] = -\ 0.0061 \cdot f\ [\%] + 0.6237\ [mm] \qquad (12)$$

For implementation in the height control strategy, equation 13 is derived from equation 12. It describes the relation between feed rate and local height deviations. Local height deviation is divided by four, because the LLS measurements of the deposited height are conducted every four layers within the first implementation of the height control strategy.

$$f_i \left[\frac{m}{s}\right] = f_{Nom} \left[\frac{m}{s}\right] - 0.0546 \left[\frac{\frac{m}{s}}{mm}\right] \cdot \frac{\Delta h_{local}}{4}\ [mm] \qquad (13)$$

In experiment 5, tilted planes are deposited by reducing the feed rate from FP30 to FM30 in feed rate increments of 10% when moving the TCP in positive y-direction. Each track consists of seven feed rate segments with a length of $\Delta s = 2$ mm each. This yields, together with the contour tracks, an edge length of the deposited cuboids of 18 mm. Expected geometric features minimum height h_{min}, maximum height h_{max} and tilting angle α of the tilted plane are calculated in table 3.

Table 3. Expected geometric quantities of the tilted plane

Geometric quantity	**Equation**	**Expected value**
h_{max}	$[-0.0061 \cdot (-30) + 0.06237] \cdot 4$	3.23 mm
h_{min}	$[-0.0061 \cdot 30 + 0.06237] \cdot 4$	1.76 mm
α	$\tan^{-1}([h_{max} - h_{min}] / 18)$	4.67°

Evaluation of the measured point cloud data is conducted by evaluating each height profile obtained by the LLS on its own. All points that belong to the tilted plane are determined for each laser line. Linear regression is applied to these points to obtain the tilting angle α. Minimum and maximum height are obtained as the maximum and minimum height value of the points. An exemplary point cloud of a tilted plane is depicted in Figure 13. Points marked in orange color are used for evaluation.

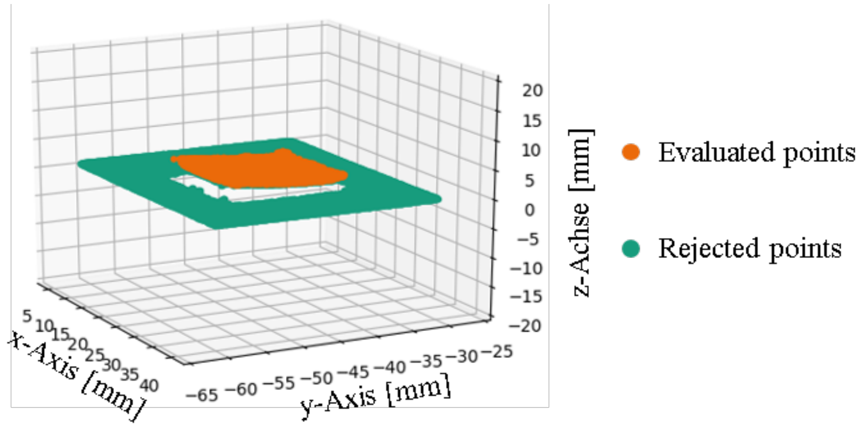

Figure 13. Evaluation of a tilted plane

Calculating the average values of each LLS measurement and each tilted plane yields an average tilting angle α = 4.428°, an average maximum height h_{max} = 2.876 mm, an average minimum height h_{min} = 1.651 mm and an average R^2-Value of 0.926. Deviation between expected and measured tilting angle is 0.242°. Geometric features of the deposited tilted planes are in good accordance with expected values.

Further deposition is conducted on top of the tilted planes to further evaluate the ability of the algorithm to compensate uneven surfaces. Single LLS line measurements of the deposition result without layer height control (Figure 14a) and of the deposition with applied layer height control (Figure 14b) are depicted in Figure 14. Set height of the deposited block is 5 mm.

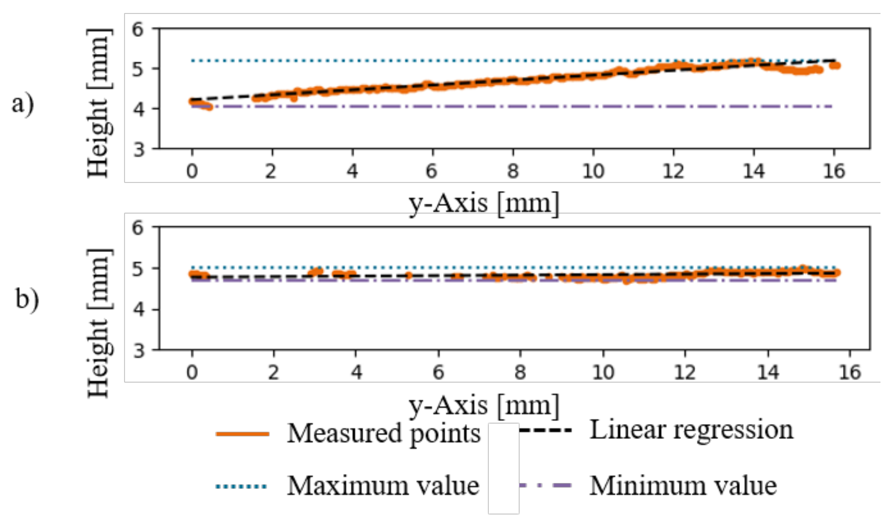

Figure 14. Comparison of controlled and uncontrolled deposition on top of the tilted plane

a) Uncontrolled deposition

b) Controlled deposition

Application of the layer height control strategy results in the tilting of the plane being almost completely leveled. On average, a resulting tilting angle of -0.389° remains. The uncontrolled deposition of another block yields a resulting tilting angle of 3.293°. The tilting of the deposited cuboid is decreased through self-stabilization of the process by 1.135° without the control algorithm. Cuboids deposited with and without layer height control strategy are shown in Figure 15.

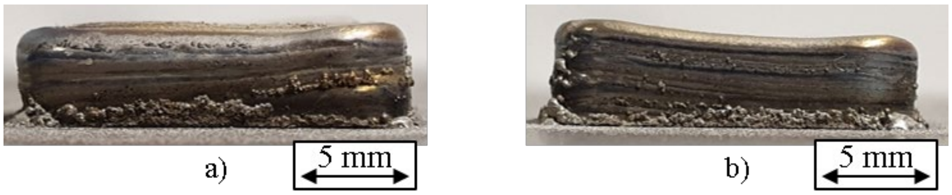

Figure 15. Cuboids deposited on tilted initial build

a) With applied layer height control strategy

b) Without applied layer height control strategy

4. CONCLUSIONS

This work presents a novel approach on process control in laser material deposition to increase stability and geometric accuracy. Previous work was extended by utilizing a laser line scanner to measure the height of deposited LMD layers. Point cloud data was processed to calculate local height deviations from a required set geometry, utilizing the random sample consensus algorithm for evaluation. Feed rate was varied along the TCP path to compensate local height deviations.

Experiments were conducted to investigate the control parameters needed for implementation of the height control strategy. Reference distance between adjacent support points on the TCP path was set to 2 mm. Maximum feed rate increment was 10%, implementation of a minimum feed rate increment was not necessary. Feed rate was varied within a ±30% interval around the nominal process feed rate. Adequate correlation between layer height and feed rate was found within this interval. Deposition experiments of cuboid specimens revealed no relevant dependency of the layer height with respect to the absolute part height.

Evaluation of the layer height control strategy was conducted by depositing tilted planes and subsequently applying the layer height control strategy to build leveled cuboids on top of them. Uncontrolled deposition on top of the tilted planes was conducted as reference. Tilted planes with a tilting angle of 4.428° were deposited, which was a deviation of only 0.242° from the expected tilting angle. Without layer height control, further deposition resulted in a final tilting angle of 3.293°. Applying the layer height control strategy yielded a remaining tilting angle of -0.389°, showing the capability to compensate uneven substrates or previously unstable process conditions.

Further work will be conducted to evaluate the performance of a layer-height controlled LMD process.. Metallurgical properties of produced parts will be investigated. Evaluation of the developed height control strategy will be conducted through experiments on specimen geometries as well as parts from industrial applications.

5. REFERENCES

[1] D. Konitzer, S. Duclos, and T. Rockstroh, “Materials for sustainable turbine engine development,” *MRS Bull.*, vol. 37, no. 4, pp. 383–387, 2012.

[2] R. Dehoff *et al.,* “Case Study: Additive Manufacturing of Aerospace Brackets,” *Advanced Materials and Processes*, vol. 171, 2013.

[3] J. M. Flynn, A. Shokrani, S. T. Newman, and V. Dhokia, “Hybrid additive and subtractive machine tools – Research and industrial developments,” *International Journal of Machine Tools and Manufacture*, vol. 101, pp. 79–101, 2016.

[4] J. I. Arrizubieta, M. Cortina, J. E. Ruiz, and A. Lamikiz, “Combination of Laser Material Deposition and Laser Surface Processes for the Holistic Manufacture of Inconel 718 Components,” (eng), *Materials (Basel, Switzerland)*, vol. 11, no. 7, 2018.

[5] F. Klocke, *Fertigungsverfahren 5*. Berlin, Heidelberg: Springer Berlin Heidelberg, 2015.

[6] I. Garmendia, J. Pujana, A. Lamikiz, J. Flores, and M. Madarieta, “Development of an Intra-Layer Adaptive Toolpath Generation Control Procedure in the Laser Metal Wire Deposition Process,” (eng), *Materials (Basel, Switzerland)*, vol. 12, no. 3, 2019.

[7] I. Garmendia, J. Leunda, J. Pujana, and A. Lamikiz, “In-process height control during laser metal deposition based on structured light 3D scanning,” *Procedia CIRP*, vol. 68, pp. 375–380, 2018.

[8] I. Garmendia, J. Pujana, A. Lamikiz, M. Madarieta, and J. Leunda, “Structured light-based height control for laser metal deposition,” *Journal of Manufacturing Processes*, vol. 42, pp. 20–27, 2019.

[9] L. Song, V. Bagavath-Singh, B. Dutta, and J. Mazumder, “Control of melt pool temperature and deposition height during direct metal deposition process,” *Int J Adv Manuf Technol*, vol. 58, no. 1-4, pp. 247–256, 2012.

[10] M. Zeinali and A. Khajepour, “Height Control in Laser Cladding Using Adaptive Sliding Mode Technique: Theory and Experiment,” *Int J Adv Manuf Technol*, vol. 132, no. 4, p. 501, 2010.

[11] A. Heralić, A.-K. Christiansson, and B. Lennartson, “Height control of laser metal-wire deposition based on iterative learning control and 3D scanning,” *Optics and Lasers in Engineering*, vol. 50, no. 9, pp. 1230–1241, 2012.

[12] H. Qi, M. Azer, and P. Singh, “Adaptive toolpath deposition method for laser net shape manufacturing and repair of turbine compressor airfoils,” *Int J Adv Manuf Technol*, vol. 48, no. 1-4, pp. 121–131, 2010.

[13] D. Hu and R. Kovacevic, “Sensing, modeling and control for laser-based additive manufacturing,” *International Journal of Machine Tools and Manufacture*, vol. 43, no. 1, pp. 51–60, 2003.

[14] M. Buhr, J. Weber, J.-P. Wenzl, M. Möller, and C. Emmelmann, “Influences of process conditions on stability of sensor controlled robot-based laser metal deposition,” *Procedia CIRP*, vol. 74, pp. 149–153, 2018.

[15] M. A. Fischler and R. C. Bolles, “Random Sample Consensus: A Paradigm for Model Fitting with Applications to Image Analysis and Automated Cartography,” *Communications of the ACM*, vol. 24, no. 6, 381-395, 1981.